AGU PUBLICATIONS

JGR

Journal of Geophysical Research: Space Physics

RESEARCH ARTICLE
10.1002/2015JA021346

Special Section:
Origins and Properties of Kappa Distributions

Key Points:
- EMIC wave instabilities in a kappa-Maxwellian are studied
- Characteristics of higher harmonics of EMIC waves are identified
- Technical description of KUPDAP dispersion solver is given

Correspondence to:
Y. Omura,
omura@rish.kyoto-u.ac.jp

Citation:
Sugiyama, H., S. Singh, Y. Omura, M. Shoji, D. Nunn, and D. Summers (2015), Electromagnetic ion cyclotron waves in the Earth's magnetosphere with a kappa-Maxwellian particle distribution, *J. Geophys. Res. Space Physics*, *120*, 8426–8439, doi:10.1002/2015JA021346.

Received 20 APR 2015
Accepted 24 AUG 2015
Accepted article online 28 AUG 2015
Published online 9 OCT 2015

Electromagnetic ion cyclotron waves in the Earth's magnetosphere with a kappa-Maxwellian particle distribution

Hajime Sugiyama[1], Satyavir Singh[1,2], Yoshiharu Omura[1], Masafumi Shoji[3], David Nunn[4], and Danny Summers[1,5]

[1]Research Institute for Sustainable Humanosphere, Kyoto University, Kyoto, Japan, [2]Indian Institute of Geomagnetism, Navi Mumbai, India, [3]Solar-Terrestrial Environment Laboratory, Nagoya University, Nagoya, Japan, [4]School of Electronics and Computer Science, University of Southampton, Southampton, UK, [5]Department of Mathematics and Statistics, Memorial University of Newfoundland, St. John's, Newfoundland, Canada

Abstract A theoretical model to study electromagnetic ion cyclotron (EMIC) waves in kappa-Maxwellian plasma is developed. The plasma is assumed to have five components, i.e., electrons, cool and hot protons, and singly charged helium and oxygen ions. The kappa-Maxwellian anisotropic particle distribution function is assumed for the hot protons. We use the Kyoto University Plasma Dispersion Analysis Package, a full dispersion solver developed at Kyoto University, to obtain the numerical results and delineate the oxygen, helium, and proton bands. Higher harmonics of the EMIC waves are also studied, and the effects of the kappa distribution on the growth of these waves are clearly demonstrated. Our results are applied to Cluster spacecraft observations of EMIC waves in the inner magnetosphere.

1. Introduction

Electromagnetic ion cyclotron (EMIC) waves are transverse, low-frequency (below the proton cyclotron frequency) waves in the range of 0.1–5 Hz and are seen on the ground as Pc1–Pc2 pulsations. EMIC waves propagating parallel to the ambient magnetic field are left-hand circularly polarized (L mode). For oblique propagation, they are coupled to right-hand circularly polarized waves (R mode). In the Earth's magnetosphere, EMIC waves play an important role in the energization and loss of magnetospheric particles. For instance, resonant pitch angle scattering by EMIC waves is thought to be a significant mechanism for inducing precipitation loss of relativistic electrons from the radiation belts [e.g., *Lorentzen et al.*, 2000; *Summers and Thorne*, 2003; *Meredith et al.*, 2003; *Summers et al.*, 2007; *Omura and Zhao*, 2013]. The primary source of free energy for the generation of EMIC waves in the inner magnetosphere is highly energetic, anisotropic ring current ions (10–100 keV) [*Cornwall*, 1965]. In the presence of protons (H^+), helium (He^+), and oxygen (O^+) ions in the magnetosphere, the observed spectrum of EMIC waves can be divided into three distinct frequency bands: H^+ band having frequency between Ω_{He} and Ω_H, He^+ band having frequency between Ω_O and Ω_{He}, and O^+ band with frequency below Ω_O, where Ω_s are the cyclotron frequencies of the respective ions. Essentially, each band of propagation is restricted by the gyrofrequency of the corresponding particle. The source region of EMIC waves is near the equator. Heavier ions such as He^+ and O^+ also play a very important role in EMIC wave generation. For example, addition of He^+ ions lowers the threshold for the excitation of these waves [*Young et al.*, 1981; *Roux et al.*, 1982; *Gomberoff and Neira*, 1983]. The observations [*Young et al.*, 1981; *Fuselier and Anderson*, 1996] and theoretical models [*Cornwall*, 1972; *Roux et al.*, 1982; *Rauch and Roux*, 1982] have shown that the presence of even a small fraction of low-energy (<1eV) He^+ can lower the EMIC instability threshold and increase the convective growth. Many authors have studied the EMIC instability in the Earth's magnetosphere [e.g., *Mauk*, 1982; *Roux et al.*, 1982; *Gomberoff and Cuperman*, 1982; *Gomberoff and Neira*, 1983; *Gendrin et al.*, 1984; *Kozyra et al.*, 1984; *Ludlow*, 1989; *Horne and Thorne*, 1993, 1994; *Hu and Fraser*, 1994] by taking the particle velocity distribution as Maxwellian.

As pointed out earlier, the main source of free energy for the excitation of EMIC waves in the inner magnetosphere is the hot ions. For example, in the case of a multicomponent ring current, during magnetic storms these ions are highly anisotropic and can lead to excitation of EMIC waves. The collisionless plasma in such regions is not in equilibrium. Therefore, particle velocity distributions are no longer Maxwellian.

These velocity distributions have power law tails [*Ipavich and Scholer*, 1983; *Ipavich et al.*, 1985] and can be well fitted by nonthermal distributions such as kappa distributions [*Christon et al.*, 1988, 1989, 1991]. The kappa distribution function was first used by *Vasyliunas* [1968] as an empirical fit to OGO1 and OGO3 solar wind data. Since then it has been successfully used to model space and magnetospheric plasmas.

The convective growth of EMIC waves modeled by a kappa particle distribution is significantly smaller than the values obtained by a bi-Maxwellian distribution function. However, during moderately disturbed conditions, substantial convective amplification can still occur in the outer magnetosphere ($L \geq 7$) [*Xue et al.*, 1996a]. Using the bi-kappa particle distribution function, the dispersive properties of obliquely propagating EMIC waves have been studied by *Xue et al.* [1996b]. It was shown that there is a possibility of excitation of high-frequency obliquely (50° – 60°) propagating EMIC waves due to the second harmonic resonance with hot anisotropic protons. *Xiao et al.* [2007] examined the EMIC wave instability driven by a temperature anisotropy of suprathermal protons. These protons were modeled with a kappa distribution in a cold multispecies plasma consisting of electrons and H^+, He^+, and O^+ ions. The EMIC instability was found to be significant above the O^+ band, and the instability threshold was found to be higher in the He^+ band than in the H^+ band. In the vicinity of the plasmapause, the effects of power law tails of the hot ring current ion velocity distribution on the growth rate and the dispersion relation for parallel-propagating EMIC waves were examined by *Mace et al.* [2011]. The presence of kappa-distributed protons significantly enhances growth rates compared to a bi-Maxwellian model. *Lazar* [2012] studied the EMIC instability and found that the lowest threshold for the instability decreases as the density of the suprathermal population increases. Recently, *Henning and Mace* [2014] have studied the effect of ion abundances on EMIC wave growth in the plasmapause region.

Researchers referenced in the previous paragraph have used bi-kappa particle distributions to study either parallel or obliquely propagating EMIC waves. To our knowledge, no attempt has been made to study obliquely propagating EMIC waves in a kappa-Maxwellian plasma. This is the first effort to study EMIC waves with a kappa-Maxwellian anisotropic particle distribution function in multicomponent magnetospheric plasma. We use KUPDAP (Kyoto University Plasma Dispersion Analysis Package), a full dispersion solver, to obtain the numerical results. This study requires the use of a special plasma dispersion function, $Z_{\kappa M}$ [*Hellberg and Mace*, 2002]. We will use observed parameters from the Cluster spacecraft in the inner magnetosphere for our theoretical model. The purpose of this study is twofold: (i) to demonstrate the EMIC wave results based on the new particle distribution, i.e., a kappa-Maxwellian distribution for hot protons, and (ii) to validate the newly developed dispersion solver KUPDAP. The manuscript is organized as follows. The theoretical model is presented in section 2, the numerical results are presented in section 3, and the conclusions are stated in section 4. A technical description of KUPDAP is given in Appendix A.

2. Theoretical Model

Hellberg and Mace [2002] proposed a physically and mathematically useful anisotropic distribution function having a one-dimensional generalized Lorentzian distribution with an arbitrary value of kappa along the ambient magnetic field and a two-dimensional Maxwellian distribution in the plane perpendicular to it. This distribution function is known as a kappa-Maxwellian distribution. The justification for such a distribution function is that there is equilibration and isotropization in the perpendicular plane and preferential acceleration along the magnetic field that leads to a power law distribution. Further, the other important physical aspect of the kappa distribution in the parallel direction is the resonant wave-particle interaction between the excited waves and the enhanced population of suprathermal charged particles that are moving along the ambient magnetic field [*Basu and Grossbard*, 2011]. *Hellberg and Mace* [2002] and *Mace and Hellberg* [2009] have developed a special dispersion function for such distributions represented by $Z_{\kappa M}$. They have also established a relationship between the dispersion function Z_κ (dispersion function for kappa distribution) and $Z_{\kappa M}$ and have discussed various other properties of this distribution function. Mathematically, $Z_{\kappa M}$ is easily tractable. Also, the kappa-Maxwellian distribution function asymptotically approaches the bi- Maxwellian distribution in the limit as $\kappa \to \infty$.

We assume an infinite, uniform, collisionless multicomponent plasma consisting of electrons, cool and hot protons (H^+), and helium (He^+) and oxygen (O^+) ions. The plasma is considered to be immersed in a uniform magnetic field $\mathbf{B_0} \parallel \hat{\mathbf{z}}$. All the species are assumed to be magnetized. The EMIC waves are assumed to propagate in the *x*-*z* plane with a wave vector $\mathbf{k} = k_x\hat{x} + k_z\hat{z}$, where $k_x = k_\perp = k\sin\theta$ and $k_z = k_\parallel = k\cos\theta$ are the perpendicular and parallel wave numbers, respectively, with $k_y = 0$. The wave vector makes an angle θ

with the ambient magnetic field $\mathbf{B_0}$. Further, we assume the electrons, cool protons, and helium and oxygen ions to have a Maxwellian velocity distribution. The hot protons, whose number density is a small fraction of the cool protons, are assumed to have a kappa-Maxwellian velocity distribution [*Hellberg and Mace*, 2002; *Cattaert et al.*, 2007]. A kappa-Maxwellian distribution for hot protons can be constructed as a product of kappa and Maxwellian distributions parallel and perpendicular to the ambient magnetic field, respectively; i.e., the parallel velocity distribution of hot protons is modeled by a kappa distribution and the perpendicular velocity distribution is modeled by a Maxwellian distribution. Further, the parallel and perpendicular temperatures are, in general, taken to be different. Thus, the hot proton distribution can be expressed as [*Hellberg and Mace*, 2002; *Cattaert et al.*, 2007]

$$f_{\kappa M}(v_\parallel, v_\perp) = h(v_\parallel) H(v_\perp) \ , \tag{1}$$

$$h(v_\parallel) = \frac{1}{(2\pi)^{1/2} V_{\kappa t\parallel}} \frac{\Gamma(\kappa)}{\sqrt{\kappa}\,\Gamma(\kappa - 1/2)} \left(1 + \frac{(v_\parallel - V_0)^2}{2\kappa V_{\kappa t\parallel}^2}\right)^{-\kappa} \ , \tag{2}$$

$$H(v_\perp) = \frac{1}{2\pi V_{t\perp}^2} \exp\left(-\frac{v_\perp^2}{2V_{t\perp}^2}\right) \ , \tag{3}$$

where $V_{t\perp} = \sqrt{T_\perp/m_\mathrm{H}}$ and $V_{\kappa t\parallel} = (1 - 3/2\kappa)^{1/2} V_{t\parallel}$ (where $V_{t\parallel} = \sqrt{T_\parallel/m_\mathrm{H}}$) are the perpendicular and effective parallel thermal speeds, respectively; m_H, $T_\parallel$, and $T_\perp$ are the mass, parallel temperature, and perpendicular temperature of the hot protons, respectively; and V_0 is the drift speed. In the limit $\kappa \to \infty$, the particle distribution $f_{\kappa M}$ reduces to the bi-Maxwellian.

The temperature anisotropy, i.e., the ratio of the two temperatures (perpendicular and parallel) is obtained by taking the second moments of the distribution function given by equations (1)–(3). Thus, the anisotropy for the kappa-Maxwellian distribution function comes out to be $A = T_\perp/T_\parallel - 1$, which is the same as for bi-Maxwellian particle distribution. For the kappa-Maxwellian distribution, the general susceptibility tensors for obliquely propagating electromagnetic waves have been derived by *Cattaert et al.* [2007] in the same geometry as has been described in the previous paragraph for the propagation of the EMIC waves. They assume that the perturbations vary as $\exp[i(\mathbf{k}.\mathbf{r} - \omega t)]$. Thus, the nine elements of the susceptibility tensor for the hot protons, which are assumed to have a kappa-Maxwellian distribution, can be written as [*Cattaert et al.*, 2007]

$$\chi_{11} = \frac{\omega_{\mathrm{pH}}^2}{\omega^2}\left(-1 + \frac{e^{-\lambda}}{\lambda}\sum_{n=-\infty}^{+\infty} n^2 I_n C_n\right) , \tag{4}$$

$$\chi_{12} = -\chi_{21} = -i\frac{\omega_{\mathrm{pH}}^2}{\omega^2} e^{-\lambda} \sum_{n=-\infty}^{+\infty} n\left(I_n - I_n'\right) C_n \ , \tag{5}$$

$$\chi_{13} = \chi_{31} = \frac{\omega_{\mathrm{pH}}^2}{\omega^2}\ \tan\theta \left(1 + \frac{e^{-\lambda}}{\lambda}\sum_{n=-\infty}^{+\infty} \frac{(\omega - n\Omega_\mathrm{H})}{\Omega_\mathrm{H}} n I_n C_n\right) \ , \tag{6}$$

$$\chi_{22} = \frac{\omega_{\mathrm{pH}}^2}{\omega^2}\left(-1 + \frac{e^{-\lambda}}{\lambda}\sum_{n=-\infty}^{+\infty} \left[n^2 I_n + 2\lambda^2\left(I_n - I_n'\right)\right] C_n\right) \ , \tag{7}$$

$$\chi_{23} = -\chi_{32} = i\frac{\omega_{\mathrm{pH}}^2}{\omega^2}\ \tan\theta\ e^{-\lambda}\left(\sum_{n=-\infty}^{+\infty} \frac{(\omega - n\Omega_\mathrm{H})}{\Omega_\mathrm{H}}(I_n - I_n')C_n\right) \ , \tag{8}$$

$$\chi_{33} = \frac{\omega_{\mathrm{pH}}^2}{\omega^2}\ \tan^2\theta \left[-1 + \frac{e^{-\lambda}}{\lambda}\sum_{n=-\infty}^{+\infty}\left(\frac{\omega - n\Omega_\mathrm{H}}{\Omega_\mathrm{H}}\right)^2 I_n C_n\right] \ , \tag{9}$$

where

$$C_n = \int_{-\infty}^{+\infty} \mathrm{d}v_\parallel \frac{-n\Omega_\mathrm{H} h(v_\parallel) + k_\parallel V_{t\perp}^2 h'(v_\parallel)}{\omega - k_\parallel v_\parallel - n\Omega_\mathrm{H}} \ . \tag{10}$$

Here $\omega_{pH} = \sqrt{n_H e^2/\epsilon_0 m_H}$ and $\Omega_H = eB_0/m_H$ are the plasma and gyrofrequencies of the protons, m_H is the proton mass, ϵ_0 is the permitivity, n_H is the density, and e is the charge. I_n and I'_n are the modified Bessel function and its derivative, respectively. The argument of the modified Bessel function is $\lambda = k_\perp^2 \rho^2$, and $\rho = V_{t\perp}/\Omega_H$ is the gyroradius. The integral C_n corresponding to the kappa-Maxwellian velocity distribution is given as [*Cattaert et al.*, 2007]

$$C_n = \frac{n\Omega_H}{\sqrt{2}k_\parallel V_{\kappa t\parallel}} Z_{\kappa M}(\zeta_n) - \frac{V_{t\perp}^2}{2V_{\kappa t\parallel}^2} Z'_{\kappa M}(\zeta_n) \ , \tag{11}$$

which can be substituted in (4)–(10) to obtain the elements of the susceptibility tensor χ. Here

$$\zeta_n = \frac{\omega - k_{||} V_0 - n\Omega_H}{\sqrt{2}k_{||} V_{\kappa t||}} \ , \tag{12}$$

and $Z'_{\kappa M}(\zeta_n)$ is the derivative of the kappa-Maxwellian plasma dispersion function which is defined as [*Hellberg and Mace*, 2002]

$$Z_{\kappa M}(\zeta_n) = \frac{1}{\pi^{1/2}} \frac{\Gamma(\kappa)}{\sqrt{\kappa}\,\Gamma(\kappa - 1/2)} \int_{-\infty}^{\infty} \frac{(1 + t^2/\kappa)^{-\kappa}}{t - \zeta_n} \mathrm{d}t \ . \tag{13}$$

In the limit $\kappa \to \infty$, the kappa-Maxwellian plasma dispersion function $Z_{\kappa M}(\zeta_n)$ approaches $Z(\zeta_n)$, which is the dispersion function for Maxwellian plasma [*Fried and Conte*, 1961]. Comprehensive details of the kappa-Maxwellian plasma dispersion function and its properties can be found in *Hellberg and Mace* [2002]. The kappa-Maxwellian plasma dispersion function, $Z_{\kappa M}(\zeta_n)$, can be expressed in terms of the hypergeometric function as

$$Z_{\kappa M}(\zeta_n) = i \frac{\kappa - 1/2}{\kappa^{3/2}} {}_2F_1 \left[1, 2\kappa; \kappa + 1; \frac{1}{2}\left(1 + \frac{i\zeta_n}{\sqrt{\kappa}}\right)\right] \ . \tag{14}$$

There exists a useful relationship between the kappa-Maxwellian plasma dispersion function $Z_{\kappa M}$ and the modified plasma dispersion function Z_κ, namely,

$$Z_{\kappa M}(\zeta_n) = \frac{(\kappa - 1)^{3/2}}{\kappa^{1/2}(\kappa - 3/2)} Z_{\kappa - 1}\left[\left(\frac{\kappa - 1}{\kappa}\right)^{1/2} \zeta_n \right] \ . \tag{15}$$

Further, $Z_{\kappa M}(\zeta_n)$ can be expanded in the small and large argument limits, as discussed by *Hellberg and Mace* [2002]. The power series expansion of

$Z_{\kappa M}(\zeta_n)$ in the limit $\zeta_n \ll 1$ is given by

$$Z_{\kappa M}(\zeta_n) = \frac{i\sqrt{\pi}\,\Gamma(\kappa)}{\kappa^{1/2}\Gamma(\kappa - 1/2)} \left(1 + \frac{\zeta_n^2}{\kappa}\right)^{-\kappa} - \frac{\sqrt{\pi}}{\kappa\Gamma(\kappa - 1/2)} \zeta_n \sum_{m=0}^{\infty} \left(\frac{-1}{\kappa}\right)^m \frac{\Gamma(\kappa + m + 1/2)}{\Gamma(m + 3/2)} \zeta_n^{2m} \ , \tag{16}$$

and in the limit $\zeta_n \gg 1$, the asymptotic expansion is given by

$$\begin{aligned} Z_{\kappa M}(\zeta_n) = {} & \sqrt{\pi}\, \frac{\Gamma(\kappa)\kappa^{\kappa - 1/2}}{\Gamma(\kappa - 1/2)} \left(\frac{1}{\zeta_n^2 + \kappa}\right)^{\kappa} (i - \tan(\kappa\pi)) \\ & - \sqrt{\pi}\,\Gamma(3/2 - \kappa) \sum_{m=0}^{\infty} \left(\frac{\kappa^m}{\Gamma(3/2 - \kappa + m)\Gamma(1/2 - m)} \frac{1}{\zeta_n^{2m+1}} \right) \ . \end{aligned} \tag{17}$$

It should be mentioned here that this series is divergent for half-integer values of κ. Therefore, for half-integer values of κ, the alternative asymptotic expansions developed by *Summers et al.* [1996] must be used. The modified plasma dispersion function $Z_\kappa(\zeta_n)$, corresponding to the kappa distribution for integer κ, was developed by *Summers and Thorne* [1991].

To investigate the dispersion characteristics of the waves, the dielectric tensor can be calculated by using standard procedures [*Stix*, 1992] and can be expressed as

$$\epsilon_{ij} = \delta_{ij} + \sum_s \chi_{ij,s} \ . \tag{18}$$

Here δ_{ij} is the Kronecker delta, and $\chi_{ij,s}$ refers to the susceptibility tensor of species denoted by s. In our model we take s = e, H^+, He^+, O^+, which refer to the electrons, proton, helium ion, and oxygen ion, respectively. The susceptibility tensors χ_{ij} for the Maxwellian plasma components, i.e., for the electrons, cool protons, helium ion, and oxygen ion, are taken from *Akhiezer et al.* [1975].

The dispersion relation for obliquely propagating electromagnetic waves in a hot magnetized plasma with a kappa-Maxwellian distribution can be obtained by equating the determinant of the tensor

$$\Lambda_{ij} = \frac{c^2}{\omega^2}\left(k_i k_j - k^2\delta_{ij}\right) + \epsilon_{ij} \tag{19}$$

to zero, i.e.,

$$\begin{vmatrix} \epsilon_{11} - k_\parallel^2 c^2/\omega^2 & \epsilon_{12} & \epsilon_{13} + k_\parallel k_\perp c^2/\omega^2 \\ -\epsilon_{12} & \epsilon_{22} - k^2 c^2/\omega^2 & \epsilon_{23} \\ \epsilon_{13} + k_\parallel k_\perp c^2/\omega^2 & -\epsilon_{23} & \epsilon_{33} - k_\perp^2 c^2/\omega^2 \end{vmatrix} = 0 \ . \tag{20}$$

3. Numerical Results

The numerical results presented in this paper are obtained using the Kyoto University Plasma Dispersion Analysis Package (KUPDAP), which is a dispersion solver developed by the Space Group at Kyoto University, Kyoto, Japan. KUPDAP takes into account a multicomponent, infinite, uniform, collisionless plasma immersed in a uniform magnetic field. A given electromagnetic dispersion relation is solved using the secant method [*Allen and Isaacson*, 1998] for finding the roots of the polynomial equation. This method uses a succession of roots of secant lines to better approximate a root of a given function. A graphic user interface (GUI) has been developed using the GTK+ library. The source codes of KUPDAP are written in the programming language C which is compatible with GTK+ library. The input parameters can be provided to KUPDAP either as absolute values or in a certain prescribed format. The dispersion solver "Waves in Homogeneous Anisotropic Magnetized Plasma" (WHAMP) [*Ronnmark*, 1982] was developed many years ago, but KUPDAP has two advantages over WHAMP. First, KUPDAP calculates the plasma dispersion function by Gautschi's method [*Gautschi*, 1970] which yields an accuracy of up to 10 significant digits, while WHAMP uses the Padé approximation, which gives an absolute error up to 3×10^{-6}. Therefore, KUPDAP obtains a more accurate solution. Second, KUPDAP can obtain all the dispersion curves simultaneously unlike WHAMP. KUPDAP has another unique feature in that not only can it solve a dispersion relation for Maxwellian, bi-Maxwellian, and subtracted Maxwellian particle distributions but also for kappa-Maxwellian particle distributions. This requires the use of the special dispersion function $Z_{\kappa M}$ [*Hellberg and Mace*, 2002]. The characteristics of a given wave can also be analyzed for angles of propagation from 0° to 90°. Further details regarding KUPDAP are provided in Appendix A in this paper.

For the numerical computation of EMIC wave dispersion properties in a hot kappa-Maxwellian distribution, the dispersion relation (20) will be analyzed for obliquely propagating waves. The parameters for EMIC wave dispersion have been taken from Cluster spacecraft observations in the inner magnetosphere [*Omura et al.*, 2010; *Pickett et al.*, 2010]. For the first time, Cluster observed EMIC wave triggered emissions associated with Pc1 waves near the Earth's plasmapause at $L = 4.3$ on 30 March 2002. During this event, the Waves of High frequency and Sounder for Probing of Electron density by Relaxation and Electric Field and Wave Experiment instruments on board the Cluster spacecraft measured the electron density, $n_e = 178/\text{cm}^3$. The observations showed the presence of H^+, He^+, and O^+ ions, and their plasma densities were estimated to be $n_H = 144/\text{cm}^3$, $n_{He} = 17/\text{cm}^3$, and $n_O = 17/\text{cm}^3$, respectively. The observations also revealed the presence of hot anisotropic H^+ ions during the entire interval of the wave observations. Their densities were estimated to be 5% of the total proton population. The perpendicular and parallel thermal speeds for the hot anisotropic protons are taken to be $V_{t\perp} = 800$ km/s and $V_{t\parallel} = 600$ km/s, respectively. The proton cyclotron frequency is estimated to be $f_H = 3.7$ Hz. The values of kappa assumed in this study are specified in the figures. The observed values of κ are reported to be in the range 2–6 [*Xue et al.*, 1996b]. The parameters used in the numerical computations are given in Table 1.

Figure 1a shows the variation of normalized frequency (ω/Ω_H) and growth rate (γ/Ω_H) versus normalized wave number $k\rho_H$ for the observed parameters in the plasmapause region [*Omura et al.*, 2010; *Pickett et al.*, 2010] and for an angle of propagation, $\theta = 0°$ and $\kappa = 2$. Here $\rho_H = v_{tc}/\Omega_H$ is the Larmor radius and

Table 1. Plasma Parameters Related to the Cluster Observations of Electromagnetic Ion Cyclotron (EMIC) on 30 March 2002 in the Plasmapause Region [*Omura et al.*, 2010; *Pickett et al.*, 2010]

Species	Density (cm^{-3})	$T_{\parallel}$ (eV)	$T_{\perp}$ (eV)	Particle Distribution
H^+ (cool)	136.8	1	1	Maxwellian
H^+(hot)	7.2	3760	6700	kappa-Maxwellian
He^+	17	1	1	Maxwellian
O^+	17	1	1	Maxwellian
e^-	178	1	1	Maxwellian

$v_{tc} = \sqrt{T_c/m_H}$ is the thermal speed of the cool protons, respectively. For parallel propagation three distinct L modes, namely, O^+ mode (gray curve), He^+ mode (blue curve), and H^+ mode (red curve)) are clearly seen (Figure 1a) together with the R mode (yellow curve). The first and second crossover frequencies for these parallel-propagating waves are $f_{cr1} = 0.635$ Hz and $f_{cr2} = 1.74$ Hz, respectively. In Figures 1a–1c (top row) and 2a–2c (top row), the lower and upper black lines represent the first and second crossover frequencies and are marked as $\omega_{cr1}/\Omega_H = 0.174$) and $\omega_{cr2}/\Omega_H = 0.471$, respectively. From Figure 1a (bottom), it is very clear that the R mode (yellow curve) is unstable with the largest growth rate. The proton (red curve) and oxygen (gray curve) band L modes are stable, whereas the He^+ band (blue curve) has marginal growth in the wave number ranges $1.02 \times 10^{-2} < k\rho_H < 1.29 \times 10^{-2}$. The peak normalized growth rate (γ/Ω_H) for the R mode is 8.96×10^{-3} which occurs at $k\rho_H \approx 4.47 \times 10^{-3}$, whereas for the L mode He^+ band is 1.65×10^{-4}, which is significantly lower and occurs at $k\rho_H \approx 1.17 \times 10^{-2}$. The R mode is unstable for small wave number values, whereas the growth of L mode occurs at larger wave number values. In the case of the bi-Maxwellian proton distribution, the R mode was found to be stable (not shown here graphically), whereas the other three L modes were unstable with the helium branch having the largest growth rate. *Xue et al.* [1996a, 1996b] studied parallel and obliquely propagating EMIC waves in the Earth's magnetosphere using bi-kappa distribution for hot protons. They found that in the bi-kappa hot proton distribution case the growth rate is significantly lower than in the bi-Maxwellian distribution case. In our study of EMIC waves with a kappa-Maxwellian proton distribution, the L mode waves in the proton and oxygen bands are found to be stable for $\kappa = 2$, whereas He^+ band waves have marginal growth. These results are similar to the findings of *Xue et al.* [1996a, 1996b].

On the other hand, the R mode waves are unstable with significant growth rate. It is interesting to note that in the earlier studies, the R mode wave has been excited with a negative proton anisotropy. For example, the growth of ion cyclotron whistlers in the solar wind is associated with proton anisotropy. These R mode

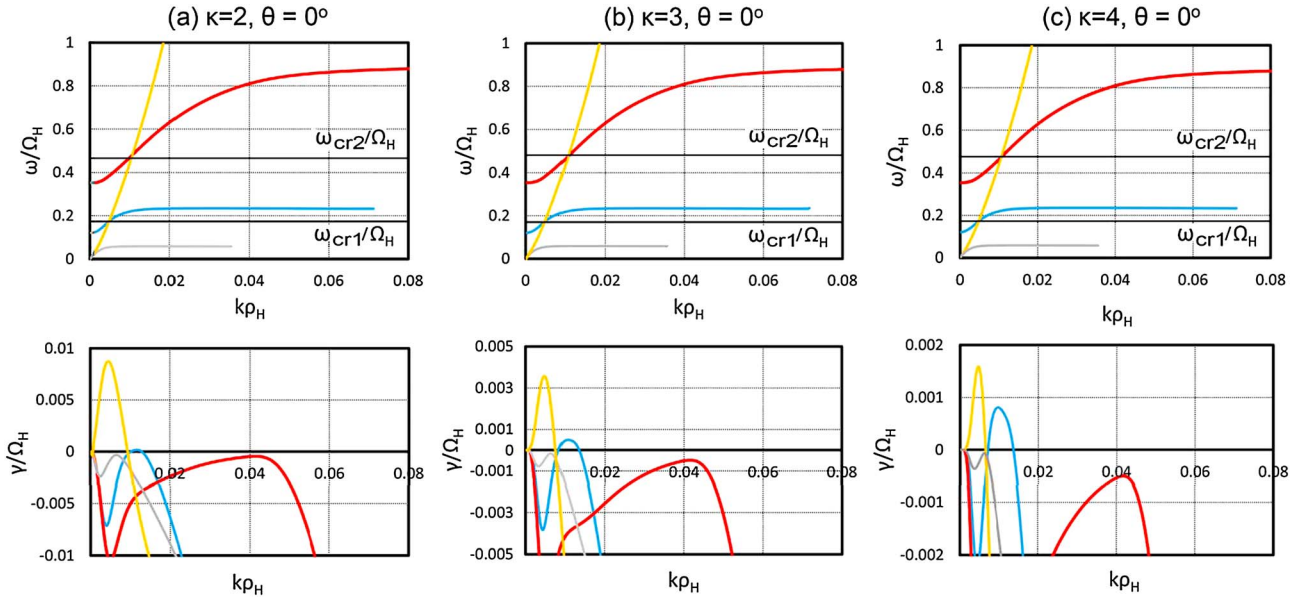

Figure 1. (top row) Frequencies and (bottom row) corresponding growth rates for $\theta = 0°$. R mode (yellow), L modes, proton band (red), He^+ band (blue), and O^+ band (gray): (a) $\kappa = 2$, (b) $\kappa = 3$, and (c) $\kappa = 4$.

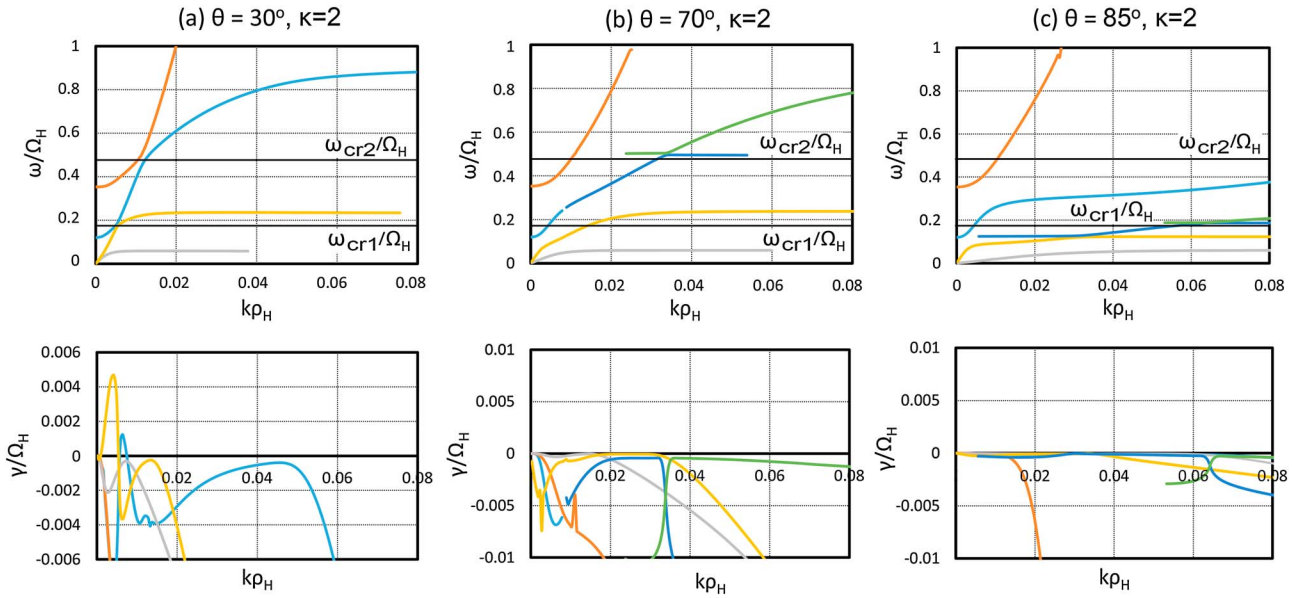

Figure 2. (top row) Frequencies and (bottom row) corresponding growth rates for $\kappa = 2$: (a) $\theta = 30°$, (b) $\theta = 70°$, and (c) $\theta = 85°$.

low-frequency electromagnetic waves are excited when the parallel temperature of the protons is larger than the perpendicular temperature, thus giving a negative anisotropy [*Scarf and Fredricks*, 1968]. *Xue et al.* [1993] have shown the growth of R mode EMIC waves with anisotropic protons modeled by a kappa distribution. The R mode waves were generated using $T_{\parallel} = 5T_{\perp}$ (cf. Figure 2). Since these authors did not consider a multicomponent plasma, it is not clear whether He^+ band waves could have positive growth rates. Further, it was shown that bi-Lorentzian protons with an anisotropy, $T_{\parallel} > T_{\perp}$, can provide significant local convective amplification of R mode compressional Alfven waves for small angles ($\theta < 20°$) of propagation to the magnetic field [*Xue et al.*, 1996c]. In this study, however, the perpendicular temperature is larger than the parallel temperature for hot protons, and the anisotropy is positive. It is emphasized that the kappa-Maxwellian proton distribution with the positive anisotropy can excite R mode waves.

Figure 1b shows the normalized frequency and growth rates for $\kappa = 3$, and Figure 1c shows the normalized frequency and growth rates for $\kappa = 4$ for parallel-propagating EMIC waves. It is evident from Figure 1 that the frequency of the R mode as well as the L modes is not affected by the variation of κ. The growth rate of these R mode waves decreases as κ is increased from 2 to 4 (Figure 1, bottom row). This may be because as κ values increase, the hot proton distribution will be closer to the Maxwellian distribution and hence will be depleted of its energy to sustain the wave growth. The range of wave numbers for which the R mode is found to be unstable also decreases with an increase in κ values. However, for the L mode He^+ band waves the growth rate increases as κ increases. Also, the range of wave numbers for which these waves are unstable increases as κ increases. Thus, our results on generation of L mode EMIC instability based on kappa-Maxwellian proton distribution are similar to the results of *Xue et al.* [1996a, 1996b]. Further, the growth rate is smaller for the L mode He^+ band waves than for the R mode waves. The R mode waves are more unstable for lower wave number ranges than the L mode He^+ band waves.

Mace et al. [2011] have studied the growth of parallel-propagating EMIC waves generated exclusively by hot ions with a bi-kappa distribution. Their results show that the He^+ branch of the instability has the highest growth rate (cf. lower panel of Figure 1 of *Mace et al*. [2011]), and the real frequency of any EMIC wave branch is unaffected by a variation of the κ index (cf. upper panels of Figures 2, 3, and 4 of *Mace et al.* [2011]). For comparison with our results, we examine the He^+ branch of the EMIC waves as described by *Mace et al.* [2011]. They have shown that the growth rate of this branch maximizes at $\kappa = 2$ and thereafter decreases with an increase in κ value (cf. lower panel of Figure 3 of *Mace et al.* [2011]). Further, we notice that the range of wave numbers for which EMIC wave instability is obtained increases with an increase in κ value. We compare our results qualitatively with *Mace et al.* [2011]. Figure 1 (top row) shows the normalized real frequency versus $k\rho_H$ for $\kappa = 2, 3, 4$, respectively, for parallel-propagating EMIC waves. The real frequency does not show any dependence on the parameter κ. Further, the growth rates change significantly with increase in κ values

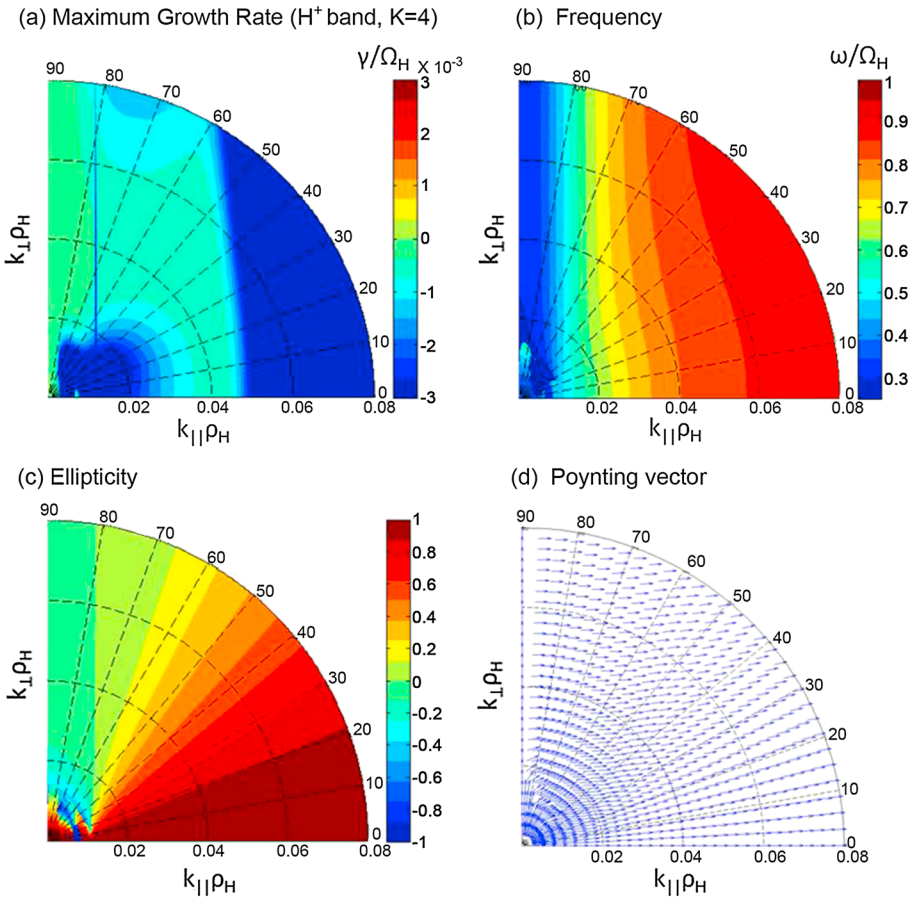

Figure 3. (a) Maximum growth rate in H^+ band ($\omega = 0.25–1.0\ \Omega_H$) for $\kappa = 4$ and $\theta = 0–90°$ and corresponding (b) frequency, (c) ellipticity, and (d) Poynting vector.

from 2 to 4. The peak growth rate as well as the window for growing wave numbers for the L mode He^+ band waves increases with an increase in κ values. These results are consistent with the results obtained by *Mace et al.* [2011]. The only difference is that in the *Mace et al.* [2011] study the growth rate maximizes at $\kappa = 1.6$, which is not allowed in our case since only integer κ values can be used as a result of the assumed mathematical form of the dispersion function $Z_{\kappa M}$. For the R mode waves, our results show that the peak growth rate decreases and the range of growing wave numbers decreases with an increase in κ values. These results are again qualitatively similar to the findings of *Mace et al.* [2011] in their study of the parallel whistler instability excited by the electrons with a bi-kappa distribution.

Next, we examine the case of wave propagation at $\theta = 30°$ for the parameters mentioned in the previous paragraph and for $\kappa = 2$. Here the coupling between the R mode and L mode can be seen in Figure 2a. The corresponding normalized growth rates are plotted in Figure 2a (bottom). The two peaks in the growth rate appearing in Figure 2a (bottom) correspond to the unstable R mode waves. The first peak shows the unstable R mode waves below the first crossover frequency $f_{cr1} = \omega_{cr1}/2\pi \approx 0.635$ Hz that corresponds to $\omega/\Omega_H = 0.174$ for wave numbers $k\rho_H \leq 5.4\times10^{-3}$. This mode is stable for frequencies $\omega > \omega_{cr1}$. The second peak corresponds to unstable R mode waves between the first crossover frequency ω_{cr1} and the He^+ gyrofrequency but has a smaller peak growth rate compared to the R mode waves below the crossover frequency. It is stable above the frequencies $\omega > \Omega_{He}$. The three L mode waves are damped modes.

Now we explore the dispersive properties of EMIC waves at more oblique angles. From numerical results (not shown here), we find that for $\kappa = 2$ and $\theta \leq 53°$, the R modes are unstable whereas L modes are damped modes. Thus, R modes are unstable for fairly oblique angles of propagation. However, further increase in obliquity gives interesting results at $\theta = 70°$. There appears a second harmonic of He^+ at $\omega = 2\Omega_{He}$, i.e., $\omega = 0.5\Omega_H$ for wave numbers $0.024 \leq k\rho_H \leq 0.054$ which is represented by the green-blue horizontal line in

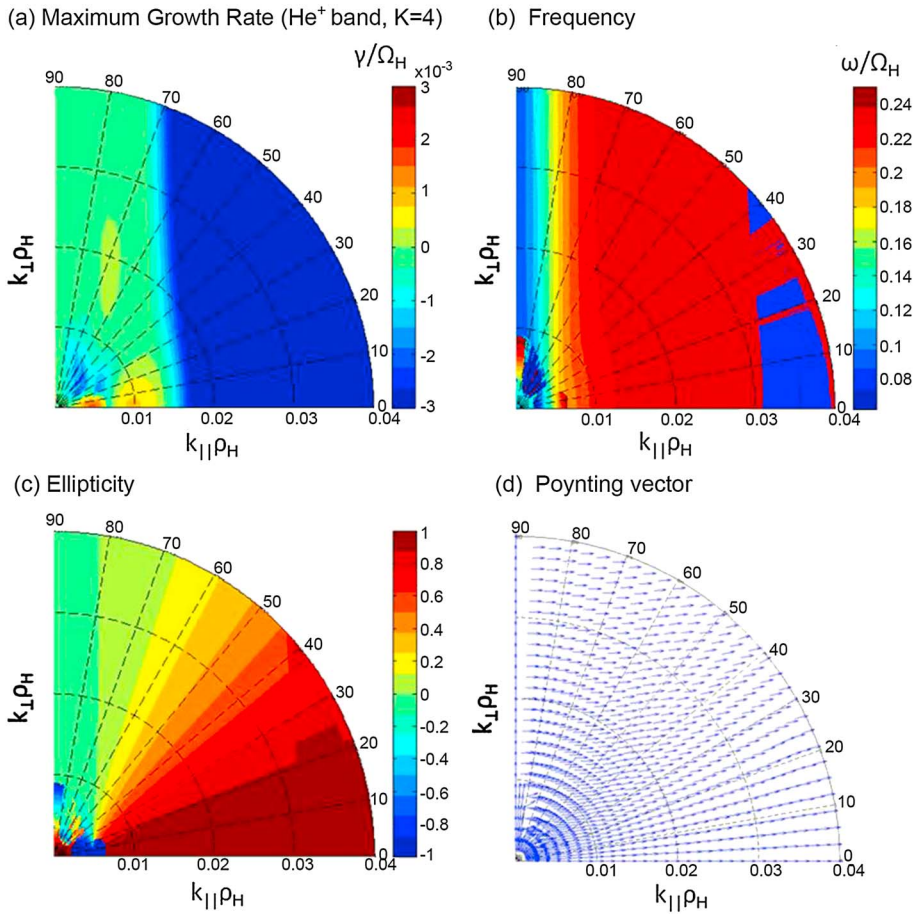

Figure 4. (a) Maximum growth rate in He^+ band ($\omega = 0.0625–0.25\ \Omega_H$) for $\kappa = 4$ and $\theta = 0–90°$ and corresponding (b) frequency, (c) ellipticity, and (d) Poynting vector.

Figure 2b. The polarization of these waves is mixed; i.e., for wave numbers $0.024 \leq k\rho_H \leq 0.034$, the polarization is right handed, whereas for $k\rho_H \geq 0.034$, it is left handed. The second harmonic of helium is similar to that obtained in the case of bi-Maxwellian plasmas and appears due to the resonant interaction between the waves and He^+ ions. Further, at $\theta = 85°$ (Figure 2c), absorption takes place at $\omega = 2\Omega_O$ for wave number ranges $0.005 \leq k\rho_H \leq 0.08$ (the blue-yellow horizontal curve in Figure 2c (top)) and at $\omega = 3\Omega_O$ for wave number ranges $0.053 \leq k\rho_H \leq 0.08$ (the green horizontal curve in Figure 2c (top)). In the case of second harmonic of oxygen the polarization is right handed for $0.005 \leq k\rho_H \leq 0.048$ and left handed for $k\rho_H > 0.048$. Similarly, for third harmonic of oxygen waves are right handed for wave numbers $0.053 \leq k\rho_H \leq 0.067$ and left handed for $k\rho_H > 0.067$. This implies that due to strong absorption at the second harmonic of helium and the second and third harmonics of oxygen, the heavier ions can be heated in a direction perpendicular to the ambient magnetic field. The corresponding damping rates for $\theta = 70°$ and $85°$ are plotted in Figures 2b (bottom) and 2c (bottom), respectively. For oblique propagation of EMIC waves our results on harmonic resonance at the He^+ cyclotron frequency are consistent with those of *Xue et al.* [1996b] and *Zhang et al.* [2011], while our results on harmonic resonance at the O^+ ion cyclotron frequency are consistent with the findings of *Thorne and Horne* [1994]. Further, our numerical computations show that electron Landau damping is not important for angle of propagation, $\theta < 30°$, but becomes significant at large angles of propagation. Also, an increase in the electron temperature adversely affects the growth of the waves at large angles of propagation. This is similar to the results obtained by *Ludlow* [1989] for EMIC waves driven by anisotropic protons in the magnetosphere.

In Figure 3, we have plotted the maximum normalized growth rates (Figure 3a), normalized frequency (Figure 3b), ellipticity (Figure 3c), and Poynting vectors (Figure 3d), respectively, for H^+ band EMIC waves for $\kappa = 4$ and $\theta = 0°–90°$. We briefly describe how the normalized maximum growth rates are obtained.

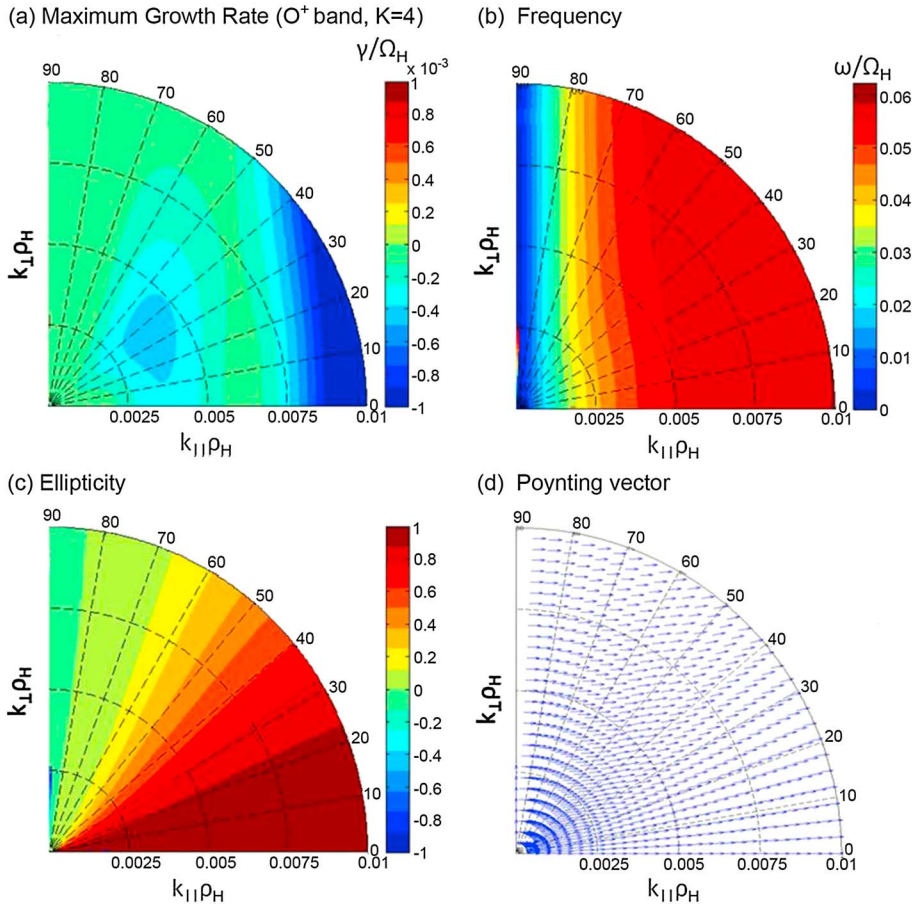

Figure 5. (a) Maximum growth rate in O^+ band ($\omega = 0.0-0.0625\ \Omega_H$) for $\kappa = 4$ and $\theta = 0-90°$ and corresponding (b) frequency, (c) ellipticity, and (d) Poynting vector.

First, growth rates are calculated for each angle of propagation between $\theta = 0°$ and 90° at an interval of 1° for the range of wave numbers and the set of parameters described in Table 1. Thereafter, the maximum growth rates are chosen for each angle of propagation and are normalized with respect to the proton cyclotron frequency. The wave numbers are normalized with respect to the cool proton gyroradius. Contour plots are constructed for the maximum normalized growth rates for each angle of propagation from $\theta = 0°$ to 90° as shown in Figures 3a, 4a, and 5a. On the horizontal and vertical axes, we plot the parallel ($k_{\|}\rho_H$) and perpendicular ($k_{\perp}\rho_H$) normalized wave numbers. In Figure 3a, the blue vertical line corresponds to the second harmonic at the helium gyrofrequency that appears at $\theta = 70°$, as discussed in the previous paragraph. Figure 3c shows the ellipticity of the H^+ band which is indicative of the polarization of the waves. The bar on the right-hand side of Figure 3c shows the values of the ellipticity varying from −1 to +1. Here −1 represents left-handed polarization, +1 represents the right-handed polarization, and "0" indicates linearly polarized waves. This general representation of ellipticity is the same for the subsequent Figures 4c and 5c for the He^+ and O^+ bands, respectively. The Poynting vector direction which gives the direction of energy propagation of electromagnetic waves is plotted in Figure 3d for H^+ band EMIC waves. In Figures 4d and 5d, the Poynting vector directions are plotted for He^+ and O^+ band EMIC waves, respectively. From the results shown in Figures 3d, 4d, and 5d, it is evident from the Poynting vector directions that the energy of EMIC waves propagates almost parallel to the ambient magnetic field. The He^+ band EMIC waves are presented in Figure 4 in the same manner as that described above for Figure 3. A weak instability is found around $k_{\|}\rho_H = 0.005$ in the parallel direction, and the corresponding ellipticity (Figure 4c) shows right-handed polarization (R band waves). Further, L band unstable EMIC waves are found for small wave number ranges in the vicinity of $k_{\|}\rho_H = 0.01$ and the waves are damped for $k_{\|}\rho_H \geq 0.014$. The growth rate of the He^+ band is significantly reduced compared to the bi-Maxwellian case. It is pointed out here that in Figure 4b around $k\rho_H \geq 0.03$ which may appear discontinuous to the readers; however, the computations reveal that there is no numerical discontinuity. Further, in Figure 5, the growth

rate, frequency, ellipticity, and Poynting vector direction are plotted for O^+ waves. In this band the waves are found to be damped modes for the entire range of wave numbers unlike the bi-Maxwellian case where the waves have finite growth in the parallel direction. This implies that a kappa-Maxwellian distribution of hot protons has an adverse effect on L mode EMIC waves; i.e., the growth rate decreases in the presence of kappa-Maxwellian hot protons.

4. Conclusions

We have analyzed the dispersion relation of obliquely propagating EMIC waves in a five-component plasma comprising electrons, cool and hot protons, and helium and oxygen ions. The electrons, cool protons, and helium and oxygen ions are assumed to be Maxwellian. For the first time, EMIC instability is studied in a kappa-Maxwellian distribution for hot protons. To carry out the numerical calculations, we have utilized the Kyoto University Plasma Dispersion Analysis Package (KUPDAP). Our results show that for parallel propagation three distinct L modes (O^+, He^+, and H^+) together with the R mode are generated. The new and surprising result is that the R mode has the largest growth rate as compared to the L modes. The proton and oxygen band L modes are stable, whereas the He^+ band has marginal growth. For oblique propagation ($\theta = 70°$), no unstable mode was found and the corresponding ellipticity is linear or weakly right handed. We observed the second cyclotron resonance of helium in the proton band. Furthermore, we also found the second and the third oxygen cyclotron resonances for more oblique propagation ($\theta = 85°$). The results for oblique propagation are similar to the existing studies on EMIC waves [*Xue et al.*, 1996b].

Appendix A: Kyoto University Plasma Dispersion Analysis Package (KUPDAP)

Kyoto University Plasma Dispersion Analysis Package (KUPDAP) is a dispersion solver developed by the Space Group at the Research Institute for Sustainable Humanosphere, Kyoto University, Kyoto, Japan. It assumes a multicomponent, infinite, uniform, collisionless plasma immersed in a uniform magnetic field.

The general dispersion relation for such a plasma can be obtained by setting $|\mathbf{H}(\omega, \mathbf{k})| = 0$, where $\mathbf{H}(\omega, \mathbf{k})$ is the matrix $\mathbf{H}$ of nine elements given by

$$\mathbf{H} = \begin{pmatrix} H_1 & iH_2 & H_3 \\ -iH_2 & H_4 & -iH_5 \\ H_3 & iH_5 & H_6 \end{pmatrix} , \tag{A1}$$

$$H_1 = 1 - \frac{k_{||}^2 c^2}{\omega^2} + \chi_{11} , \tag{A2}$$

$$H_2 = -i\chi_{12} , \tag{A3}$$

$$H_3 = \frac{k_\perp k_{||} c^2}{\omega^2} + \chi_{13} , \tag{A4}$$

$$H_4 = 1 - \frac{k^2 c^2}{\omega^2} + \chi_{22} , \tag{A5}$$

$$H_5 = -i\chi_{23} , \tag{A6}$$

$$H_6 = 1 - \frac{k_\perp^2 c^2}{\omega^2} + \chi_{33} , \tag{A7}$$

where the susceptibilities χ_{ij} are given by equations (4)–(9). The technical details of the KUPDAP are given below.

A1. Roots of the Dispersion Relation

As described above, the dispersion relation for a plasma can be obtained by solving $|\mathbf{H}(\omega, \mathbf{k})| = 0$. Initially, the value of wave number k is fixed. The secant method is used to obtain the roots of the dispersion equation $|\mathbf{H}(\omega, \mathbf{k})| = 0$. Thus, we have

$$\omega_{j+1} = \frac{H_j \omega_{j-1} - H_{j-1}\omega_j}{H_j - H_{j-1}} \ . \tag{A8}$$

The search for a solution is successful if $\Delta\omega/|\omega| < 10^{-7}$; otherwise it fails when the iteration of the process exceeds 100. Thus, the search for solutions continues for each subsequent k value with an increment of the wave number $(k_{\max} - k_{\min})/200)$, and we thus obtain a dispersion curve.

A2. Initial Values

It is very important to provide initial values for the real frequencies and growth rates in order to obtain the dispersion curves. Therefore, we must know in advance where the solutions lie. Multiple initial values are used to obtain all the solutions. Initially, the search for solutions is confined to $(\omega_{r\min} - \omega_{r\max})$, $(\omega_{i\min} - \omega_{i\max})$, and $(k_{\min} - k_{\max})$. The intervals along ω_r axis, ω_i axis, and k axis are divided into $N_{\omega r}$, $N_{\omega i}$, and N_k blocks, respectively. These initial values are used at each lattice point at which KUPDAP applies the method described in section A1 to obtain dispersion curves simultaneously.

A3. Usage and Input Parameters

The source codes of KUPDAP are written in the programming language C which is compatible with the GTK+ library. Hence, the GUI is also developed. The program is supported in both Windows and Linux. The input parameters can be provided to KUPDAP either as absolute values or in a certain prescribed format. Before we proceed further, it is important to understand the meaning of each input parameter as explained below: Note that the parameters for KUPDAP are distinguished from actual values by a hat symbol.

1. c: Speed of light.
2. Ω_1: Gyrofrequency of species 1. KUPDAP computes the magnitude of the static magnetic field B_0 from the relation $B_0 = \Omega_1/(q/m)_1$.
3. θ: Angle of propagation in degrees; angle between B_0 and the wave vector $\mathbf{k}$.
4. species: Species of particle, e.g., cold, hot, or beam. You can change information of characteristic parameters of the species on PARTICLE area from this dropdown box.
5. distribution type: Chosen distribution for a particular species. From the dropdown box, one can choose bi-Maxwellian, subtracted Maxwellian, kappa-Maxwellian, or subtracted kappa-Maxwellian.
6. q: Charge. $\hat{q}_s = q_s/q_1 \times \hat{q}_1$.
7. q/m: Charge to mass ratio. $\hat{q}/\hat{m} = (q/m)_s/(q/m)_1 \times (\hat{q}/\hat{m})_1$.
8. Π or $-N$: Plasma frequency Π_s of species s. From this value, KUPDAP calculates the ratio of the density and permittivity of vacuum n_s/ϵ_0. $\hat{\Pi}_s = (\Pi_s/\Omega_1) \times \hat{\Omega}_1$. Note that you should give a positive value for species 1. For subsequent species, a negative value should be given as a density ratio to that of species 1.
9. v_{drift}: Parallel drift velocity. $\hat{V}_0 = (V_0/c) \times \hat{c}$.
10. $v_\perp$: Perpendicular thermal speed for Maxwellian, perpendicular thermal effective speed for subtracted Maxwellian. $\hat{v}_\perp = (v_{t\perp}/c) \times \hat{c}$.
11. $v_\parallel$ Parallel thermal speed for Maxwellian or parallel thermal effective speed for kappa distribution. $\hat{v}_{t\parallel} = (v_{t||}/c) \times \hat{c}$.
12. κ: $2 \leq \kappa < 128$. Note that this option is valid for kappa-Maxwellian or subtracted kappa-Maxwellian distributions.
13. b: $0 < b < 1$. It should be used for subtracted Maxwellian or subtracted kappa-Maxwellian.
14. ρ: $0 < \rho \leq 1$. It should be used for subtracted Maxwellian or subtracted kappa-Maxwellian.
15. $\omega_{r\min}$, $\omega_{r\max}$: Lower and upper bounds of real frequencies for initial solutions $\omega_{r\min}$, $\omega_{r\max}$.
16. $\omega_{i\min}$, $\omega_{i\max}$: Lower and upper bounds of imaginary frequencies for initial growth rates $\omega_{i\min}$, $\omega_{i\max}$.
17. $k_{\min}$, $k_{\max}$: Lower and upper bounds of wave numbers for initial solutions $k_{\min}$, $k_{\max}$.
18. $N_{\omega r}$, $N_{\omega i}$, N_k: Number of grids in real and imaginary frequencies and wave numbers.

KUPDAP has the unique feature that not only can it solve the dispersion relation for the Maxwellian, bi-Maxwellian, and subtracted Maxwellian particle distributions but also for kappa-Maxwellian particle distributions which require the use of the special dispersion function $Z_{\kappa M}$ [*Hellberg and Mace*, 2002]. Wave characteristics can also be analyzed for angles of propagation from 0° to 90°.

The input file can be uploaded through *File* option in the main menu in GUI, or parameters can be given directly. Once a file is uploaded, appropriate choice of distribution type should be made and the dispersion plots can be obtained by clicking the *Plot dispersion curves* button. A separate window will be displayed with upper left, lower left, and upper right panels showing $\omega_r - k$, $\omega_i - k$, and $\omega_i - \omega_r$ diagrams, respectively. In this window, several options are available. For example, clicking on the *LINES* button will show a small window with check boxes which represent all curves as numbered curves. One can hide a line by unchecking a box which has the same number as the line. Alternatively, one can hide a line by clicking near it. This function is available when the *DEL* toggle button in the lower right is checked.

To change the ranges, edit the ranges of frequency, growth rate, and wave number in the lower right. Then click the *APPLY RANGE* button.

When the *NORMALIZE* button is pushed, a separate window emerges. The first line relates to the normalization of frequency and growth rate. You can choose gyrofrequency or plasma frequency of any species you desire to normalize with. If you do not intend to normalize the frequency, choose 1. The second line refers to normalization of wave number. If you prefer $k_{||}$ or $k_{\perp}$ to k, then you should select it from the left pulldown box. You can normalize wave number by gyroradius ($\rho = v_{t\perp}/\Omega_1$) from the right pulldown box. Gyrofrequency and gyroradius depend on the species of particle and thermal velocity. Thus, one must specify the *name* of species you want to normalize within the last line.

Data created for the dispersion curves can be saved by clicking *OUTPUT* button. Unchecked lines are not saved; therefore, one should keep the desired curves for their use. The format of the output has 15 columns of k, ω_r, ω_i, and components of the matrix equation (A1) in order. Each curve is delimited by a single empty line.

KUPDAP has a very good facility for generating data for creating graphs from $\theta = 0°$ to 90° to see the whole structure of dispersion relation. However, there are many solutions at a fixed wave number. Thus, this function selects the solution which has the maximum growth rate for a certain angle of propagation. The program then repeats this procedure from $\theta_{\min}$ to $\theta_{\max}$. The boxes on the first line refer to $\theta_{\min}$, $\theta_{\max}$, and N_{div}, respectively, where N_{div} is the number of divisions between $\theta_{\min}$ and $\theta_{\max}$. The number on the right end denotes the interval of each division. The second line is the prefix of files to be saved. Data will be stored in nine files named prefix_*x*.txt.

In the resulting file, *x* refers to ω, γ, k, and $h1$–$h6$ for frequency, growth rate, wave number, and H_1–H_6 components, respectively. Formats of the outputs are N_{div} rows and 600 columns, where 600 is the number of divisions from $k_{\min}$ to $k_{\max}$.

Acknowledgments

All the new data used in this paper are obtained from KUPDAP (Kyoto University Plasma Dispersion Analysis Package). The original code of KUPDAP was developed under the leadership of Hiroshi Matsumoto in the 1980s. The authors thank Satoko Nakamura and Yuko Kubota for discussions in developing KUPDAP. The program and source codes of KUPDAP can be downloaded from the website (http://space.rish.kyoto-u.ac.jp/software/) of RISH, Kyoto University. This work was partially supported by grant-in-aid 26287120 of the Ministry of Education, Culture, Sports, Science and Technology of Japan. S.S. would like to thank RISH, Kyoto University, for the warm hospitality during his visit and G.S. Lakhina for useful discussion. D.S. acknowledges support from a Discovery Grant of the Natural Sciences and Engineering Research Council of Canada.

Larry Kepko thanks Peter Yoon and another reviewer for their assistance in evaluating this paper.

References

Akhiezer, A. I., I. A. Akhiezer, R. V. Polovin, A. G. Sitenko, and K. N. Stepanov (1975), *Plasma Electrodynamics*, pp. 225–231, Pergamon Press, Oxford.

Allen, M. B., and E. L. Isaacson (1998), *Numerical Analysis for Applied Science*, p. 188, John Wiley, New York.

Basu, B., and N. J. Grossbard (2011), Ion-cyclotron instability in current-carrying Lorentzian (kappa) and Maxwellian plasmas with anisotropic temperatures: A comparative study, *Phys. Plasmas*, *18*, 092106, doi:10.1063/1.3632974.

Cattaert, T., M. A. Hellberg, and R. L. Mace (2007), Oblique propagation of electromagnetic waves in a kappa-Maxwellian plasma, *Phys. Plasmas*, *14*(8), 082111, doi:10.1063/1.2766647.

Christon, S. P., D. G. Mitchell, D. J. Williams, L. A. Frank, C. Y. Huang, and T. E. Eastman (1988), Energy spectra of plasma sheet ions and electrons from 50 eV/e to 1 MeV during plasma temperature transitions, *J. Geophys. Res.*, *93*(A4), 2562–2572, doi:10.1029/JA093iA04p02562.

Christon, S. P., D. J. Williams, and D. G. Mitchell (1991), Spectral characteristics of plasma sheet ion and electron populations during disturbed geomagnetic conditions, *J. Geophys. Res.*, *96*, 1–22, doi:10.1029/90JA01633.

Christon, S. P., D. J. Williams, D. G. Mitchell, L. A. Frank, and C. Y. Huang (1989), Spectral characteristics of plasma sheet ion and electron populations during undisturbed geomagnetic conditions, *J. Geophys. Res.*, *94*(A10), 13,409–13,424, doi:10.1029/JA094iA10p13409.

Cornwall, J. M. (1965), Cyclotron instabilities and electromagnetic emission in the ultra low frequency and very low frequency ranges, *J. Geophys. Res.*, *70*, 61–69, doi:10.1029/JZ070i001p00061.

Cornwall, J. M. (1972), Precipitation of auroral and ring current particles by artificial plasma injection, *Rev. Geophys.*, *10*(4), 993–1002, doi:10.1029/RG010i004p00993.

Fried, B. D., and S. D. Conte (1961), *The Plasma Dispersion Function*, Academic, New York.

Fuselier, S. A., and B. J. Anderson (1996), Low energy He^+ and H^+ distributions and proton cyclotron waves in the afternoon equatorial magnetosphere, *J. Geophys. Res.*, *101*(A6), 13,255–13,265, doi:10.1029/96JA00292.

Gautschi, W. (1970), Efficient computation of the complex error function, *SIAM J. Numer. Anal.*, *7*, 187–198, doi:10.1137/0707012.

Gendrin, R., M. Ashour-Abdalla, Y. Omura, and K. Quest (1984), Linear analysis of ion cyclotron interaction in a multicomponent plasma, *J. Geophys. Res.*, *89*, 9119–9124, doi:10.1029/JA089iA10p09119.

Gomberoff, L., and S. Cuperman (1982), Combined effect of cold H^+ and He^+ ions on the proton cyclotron electromagnetic instability, *J. Geophys. Res.*, *87*, 95–100, doi:10.1029/JA087iA01p00095.

Gomberoff, L., and R. Neira (1983), Convective growth rate of ion cyclotron waves in a H^+-He^+ and H^+-He^+-O^+ plasma, *J. Geophys. Res.*, *88*, 2170–2174, doi:10.1029/JA088iA03p02170.

Hellberg, M. A., and R. L. Mace (2002), Generalized plasma dispersion function for a plasma with a kappa-Maxwellian velocity distribution, *Phys. Plasmas*, *9*, 1495–1504, doi:10.1063/1.1462636.
Henning, F. D., and R. L. Mace (2014), Effects of ion abundances on electromagnetic ion cyclotron wave growth rate in the vicinity of the plasmapause, *Phys. Plasmas*, *20*, 042905, doi:10.1063/1.4873375.
Horne, R. B., and R. M. Thorne (1993), On the preferred source location for the convective amplification of ion cyclotron waves, *J. Geophys. Res.*, *98*, 9233–9247, doi:10.1029/92JA02972.
Horne, R. B., and R. M. Thorne (1994), Convective instabilities of electromagnetic ion cyclotron waves in the outer magnetosphere, *J. Geophys. Res.*, *99*, 17,259–17,273, doi:10.1029/94JA01259.
Hu, Y. D., and B. J. Fraser (1994), Electromagnetic ion cyclotron wave amplification and source regions in the magnetosphere, *J. Geophys. Res.*, *99*, 263–272, doi:10.1029/93JA01897.
Ipavich, F. M., and M. Scholer (1983), Thermal and superthermal protons and alpha particles in the Earth's plasma sheet, *J. Geophys. Res.*, *88*(A1), 150–160, doi:10.1029/JA088iA01p00150.
Ipavich, F. M., A. B. Galvin, M. Scholer, G. Gloeckler, D. Hovestadt, and B. Klecker (1985), Suprathermal O^+ and H^+ ion behaviour during the March 22, 1979 (CDAW 6), substorms, *J. Geophys. Res.*, *90*(A2), 1263–1272, doi:10.1029/JA090iA02p01263.
Kozyra, J. U., T. E. Cravens, A. F. Nagy, E. G. Fontheim, and R. S. B. Ong (1984), Effects of energetic heavy ions on electromagnetic ion cyclotron wave generation in the plasmapause region, *J. Geophys. Res.*, *89*(A4), 2217–2233, doi:10.1029/JA089iA04p02217.
Lazar, M. (2012), The electromagnetic ion-cyclotron instability in bi-kappa distributed plasmas, *Astron. Astrophys.*, *547*, A94, doi:10.1051/0004-6361/201219861.
Lorentzen, K. R., M. P. McCarthy, G. K. Parks, J. E. Foat, R. M. Millan, D. M. Smith, R. P. Lin, and J. P. Treilhou (2000), Precipitation of relativistic electrons by interaction with electromagnetic ion cyclotron waves, *J. Geophys. Res.*, *105*(A3), 5381–5389, doi:10.1029/1999JA000283.
Ludlow, G. R. (1989), Growth of obliquely propagating ion cyclotron waves in the magnetosphere, *J. Geophys. Res.*, *94*, 15,385–15,391.
Mace, R. L., and M. A. Hellberg (2009), A new formulation and simplified derivation of the dispersion function for a plasma with a kappa velocity distribution, *Phys. Plasmas*, *16*, 072113, doi:10.1063/1.3179807.
Mace, R. L., R. D. Sydora, and I. Silin (2011), Effects of superthermal ring current ion tails on the electromagnetic ion cyclotron instability in multi-ion magnetospheric plasmas, *J. Geophys. Res.*, *116*, A05206, doi:10.1029/2010JA016393.
Mauk, B. H. (1982), Helium resonance and dispersion effects on geostationary Alfven/ion cyclotron waves, *J. Geophys. Res.*, *87*, 9107–9119, doi:10.1029/JA087iA11p09107.
Meredith, N. P., R. M. Thorne, R. B. Horne, D. Summers, B. J. Fraser, and R. R. Anderson (2003), Statistical analysis of relativistic electron energies for cyclotron resonance with EMIC waves observed on CRRES, *J. Geophys. Res.*, *108*(A6), 1250, doi:10.10129/2002JA009700.
Omura, Y., J. Pickett, B. Grison, O. Santolik, I. Dandouras, M. Engebretson, P. M. E. Decreau, and A. Masson (2010), Theory and observation of electromagnetic ion cyclotron triggered emissions in the magnetosphere, *J. Geophys. Res.*, *115*, A07234, doi:10.1029/2010JA015300.
Omura, Y., and Q. Zhao (2013), Relativistic electron microbursts due to nonlinear pitch angle scattering by EMIC triggered emissions, *J. Geophys. Res. Space Physics*, *118*, 5008–5020, doi:10.1002/jgra.50477.
Pickett, J. S., et al. (2010), Cluster observations of EMIC triggered emissions in association with Pc1 waves near Earth's plasmapause, *Geophys. Res. Lett.*, *37*, L09104, doi:10.1029/2010GL042648.
Rauch, J. L., and A. Roux (1982), Ray tracing of ULF waves in a multicomponent magnetospheric plasma: Consequences for the generation mechanism of ion cyclotron waves, *J. Geophys. Res.*, *87*, 8191–8198, doi:10.1029/JA087iA10p08191.
Ronnmark, K. (1982), Waves in homogeneous, anisotropic, multicomponent plasmas, Kiruna Geophys. Inst. Rep. 179, pp. 56, Swed. Inst. of Space Phys., Univ. of Umea, Umea, Sweden.
Roux, A., S. Perraut, J. L. Rauch, C. de Villedary, G. Kremser, A. Korth, and D. T. Young (1982), Wave particle interactions near He^+ observed on board GEOS 1 and 2, 2. Generation of ion-cyclotron waves and heating of He^+ ions, *J. Geophys. Res.*, *87*, 8174–8190.
Scarf, F. L., and R. W. Fredricks (1968), Ion cyclotron whistlers in the solar wind, *J. Geophys. Res.*, *73*(5), 1747–1755.
Stix, T. H. (1992), *Waves in Plasmas*, Am. Inst. of Phys., College Park, Md.
Summers, D., and R. M. Thorne (2003), Relativistic electron pitch angle scattering by electromagnetic ion cyclotron waves during geomagnetic storms, *J. Geophys. Res.*, *108*(A4), 1143, doi:10.1029/2002JA009489.
Summers, D., B. Ni, and N. P. Meredith (2007), Timescales for radiation belt electron acceleration and loss due to resonant wave-particle interactions: 2. Evaluation for VLF chorus, ELF hiss, and electromagnetic ion cyclotron waves, *J. Geophys. Res.*, *112*, A04207, doi:10.1029/2006JA011993.
Summers, D., and R. M. Thorne (1991), The modified plasma dispersion function, *Phys. Fluids B*, *3*, 1835–1847, doi:10.1063/1.859653.
Summers, D., R. M. Thorne, and H. Matsumoto (1996), Evaluation of the modified plasma dispersion function for half-integral indices, *Phys. Plasmas*, *3*, 2496–2501, doi:10.1063/1.871967.
Thorne, R. M., and R. B. Horne (1994), Energy transfer between energetic ring current H^+ and O^+ by electromagnetic ion cyclotron waves, *J. Geophys. Res.*, *99*(A9), 17,275–17,282, doi:10.1029/94JA01007.
Vasyliunas, V. M. (1968), A survey of low-energy electrons in the evening sector of the magnetosphere with OGO 1 and OGO 3, *J. Geophys. Res.*, *73*(9), 2839–2884, doi:10.1029/JA073i009p02839.
Xiao, F., Q. Zhou, H. He, H. Zheng, and S. Wang (2007), Electromagnetic ion cyclotron waves instability threshold condition of suprathermal protons by kappa distribution, *J. Geophys. Res.*, *112*, A07219, doi:10.1029/2006JA012050.
Xue, S., R. M. Thorne, and D. Summers (1993), Electromagnetic ion-cyclotron instability in space plasmas, *J. Geophys. Res.*, *98*(A10), 17,475–17,484, doi:10.1029/93JA00790.
Xue, S., R. M. Thome, and D. Summers (1996a), Growth and damping of oblique electromagnetic ion cyclotron waves in the Earth's magnetosphere, *J. Geophys. Res.*, *101*(A7), 15,457–15,466, doi:10.1029/96JA01088.
Xue, S., R. M. Thorne, and D. Summers (1996b), Parametric study of electromagnetic ion cyclotron instability in the Earth's magnetosphere, *J. Geophys. Res.*, *101*, 15,467–15,474, doi:10.1029/96JA01087.
Xue, S., R. M. Thome, and D. Summers (1996c), Excitation of magnetosonic waves in the undisturbed solar wind, *Geophys. Res. Lett.*, *23*(18), 2557–2560, doi:10.1029/96GL02202.
Young, D. T., S. Perraut, A. Roux, C. De Villedary, R. Gendrin, A. Korth, G. Kremser, and D. Jones (1981), Wave-particle interaction near He^+ observed on GEOS 1 and 2, 1, Propagation of ion-cyclotron waves in He^+-rich plasma, *J. Geophys. Res.*, *86*, 6755–6772, doi:10.1029/JA086iA08p06755.
Zhang, J.-C., L. M. Kistler, C. G. Mouikis, B. Klecker, J.-A. Sauvaud, and M. W. Dunlop (2011), A statistical study of EMIC wave-associated He^+ energization in the outer magnetosphere: Cluster/CODIF observations, *J. Geophys. Res.*, *116*, A11201, doi:10.1029/2011JA016690.